Thick-panel Origami Cube

Yuanqing Gu [a,c], Guowu Wei [b,*], Yan Chen [a,c,†]

[a] School of Mechanical Engineering, Tianjin University, Tianjin 300350, China

[b] School of Science, Engineering and Environment, University of Salford, Salford M5 4WT, UK

[c] Key Laboratory of Mechanism Theory and Equipment Design of Ministry of Education, Tianjin University, Tianjin 300072, PR China

Abstract

This paper presents a new method for constructing a novel thick-panel origami cube. By replacing the equivalent 4*R*-spherical linkage in a four-crease zero-thickness origami vertex with a plane-symmetric Bricard linkage, the thick-panel form of a general plane-symmetric four-crease origami vertex is identified and constructed. The proposed thick-panel vertex preserves the kinematics of the original four-crease origami vertex. Then, by utilizing the proposed thick-panel vertex, a thick-panel cube is constructed based on the zero-thickness cube that was proposed in our previous work. Through mechanism decomposition, geometric constraints and kinematic properties of the corresponding integrated mechanism are investigated and formulated, which reveals the kinematic equivalence between the thick-panel and zero-thickness forms of an origami cube. In addition, a prototype of the proposed thick-panel origami cube is fabricated, verifying its kinematic properties. The proposed technique can be extended to the design and construction of thick-panel polyhedrons with potential applications in the fields such as aerospace exploration, robotics and architecture.

Keywords: Thick-panel vertex; Plane-symmetric Bricard linkage; Thick-panel cube; Kinematic equivalence.

1. Introduction

In the past two decades, interest in folded structures and mechanisms has increased dramatically, and origami-inspired structures and mechanisms have founded applications in wide areas including, to mention but a few, aerospace mechanisms and devices [1, 2], robotics [3, 4], medical devices [5], mechanical metamaterials [6, 7], energy absorption structures [8, 9], and MEMS devices [10, 11]. The traditional origami is normally made of thin and flexible paper, but when it is transformed into engineering applications, rigid origami is considered in which the facets of the crease patterns are typically rigid panels that rotate around predetermined folds (which become complaint hinges) without any tension-bend deformation during the continuous folding process

* Corresponding author. *E-mail address*: g.wei@salford.ac.uk (G. Wei)

† Corresponding author. *E-mail address*: yan_chen@tju.edu.cn (Y. Chen)

[12]. From kinematics point of view, the folding process of a rigid origami pattern is equivalent to the motion of a mechanism if facets are regarded as rigid links and crease lines as revolute joints [13], e.g., the case that four creases in a rigid origami pattern intersect at one point is kinematically equivalent to a spherical 4*R* linkage [14-16]. In general, the traditional rigid origami patterns are primarily created by idealized zero-thickness facets. In order to enhance the engineering applications of rigid origami, the thickness problem of the panels for enhancing stiffness and strength has to be overcome. Various methods have been proposed for accommodating thickness in the folding motion of thick panels [17]. Some of these techniques maintain the original kinematic model [18] of the zero-thickness origami. The tapered panels technique [19] was proposed for geometrically constructing thick panel structures that follow the kinematic behavior of the rigid origami by trimming material away from panels to avoid interference. In the offset panel technique [20, 21], offsets were used to position the panels away from the zero-thickness surface to achieve full range of angular motions. The split-vertex technique [22] added spacer panels at fold lines to accommodate thickness, as a result, a degree-four split-vertex vertex was comprised of two spherical 4*R* linkages while maintaining single-degree-of-freedom mobility. In addition, Cai [23] proposed constructing foldable plate structure with rolling joint.

Different from the methods mentioned above, spatial linkages are utilized as another kinematic model at the origami vertices to achieve the folding motion of thick-panel origami. Ku and Demaine [24] presented the doubled hinge technique for thickness accommodation by splitting each fold line into two, thus the loop of eight creases at a simple degree-four vertex can be modeled as a spatial 8*R* linkage with two independent degrees of freedom. Lang et al. [25] proposed a new approach by using designed-offset linkages to achieve rigid foldability and parallel stacking of panels, the proposed thick origami is equivalent to a multiloop eight-bar spatial mechanism that could be analyzed as separated four-bar linkages. Hoberman [26] discovered the hinge shift technique for constructing 3D structures by shifting the location of the rotational axes away from a single plane of the Miura-ori pattern; in the proposed 3D structures, each symmetric vertex is in fact a Bennett linkage [27, 28]. Chen et al. [29] developed a systematic approach for creating thick-panel origami based on the spatial linkages, where the 4*R* Bennett linkage, 5*R* Myard linkage [30] and 6*R* Bricard linkage [31] were identified to replace the equivalent spherical linkages at four-, five- and six-crease vertices of zero-thickness origami. Using this method, the kinematic properties of the original zero-thickness origami are preserved in the thick-panel origami. In addition, Zhang and Chen [32,33] proposed a novel method for constructing mobile assemblies of spatial overconstrained linkages from origami patterns with their thick-panel forms acting as the intermediate bridge.

In order to apply the zero-thickness origami cubes [34] in engineering application with rigid and thick panels, this paper for the first time presents a new approach for constructing a thick-panel origami cube by replacing the equivalent spherical 4*R* linkages at the vertices of zero-thickness origami-form mechanism with plane-symmetric Bricard linkages. The proposed thick-panel origami cube preserves the kinematic properties of the corresponding original zero-thickness rigid-origami cube. Furthermore, following the kinematic equivalence in this proposed approach, the thick-panel origami with the same geometry can reproduce motions that are identical to that of the zero-thickness origami, in which crease pattern of zero-thickness rigid origami can be potentially applied to engineering applications based on its thick-panel form.

The rest of this paper is arranged as follows. Section 2 presents a new technique for

the design of a thick-panel form for a general plane-symmetric four-crease origami vertex. Using the proposed thick-panel vertex, Section 3 presents the synthesis and analysis of a thick-panel cube based on a foldable zero-thickness rigid-origami cube [34]. Conclusions and discussion are addressed in Section 4.

2 The thick-panel form of a general plane-symmetric four-crease origami vertex

In this section, a thick-panel form of the general plane-symmetric four-crease origami vertex is constructed and presented. The proposed thick-panel origami vertex is equivalent to a plane-symmetric Bricard linkage and can preserve the kinematics of the original four-crease origami vertex.

2.1 Design of the thick-panel form for a general plane-symmetric four-crease origami vertex

A plane-symmetric four-crease zero-thickness origami vertex in the Miura-ori pattern is shown in Fig. 1(a), where the red solid lines stand for mountain creases, and the dashed lines denote valley creases. This type of origami vertex has two groups of sector sheets with section angles α and β, as indicated in blue and yellow respectively in Fig. 1. It should be noted that $\alpha+\beta=\pi$ is the geometric condition of coplanarity corresponding to Miura-ori pattern. Regarding the creases and rigid sheets as revolute joints and links, respectively, the four-crease rigid origami vertex can be modeled as a spherical 4*R* linkage of one degree-of-freedom (DOF). The corresponding thick-panel origami of this rigid origami pattern was firstly proposed by Hoberman [26] by using the hinge shift technique as shown in Fig. 1(b). This thick-panel form origami has one DOF, the thickness of thicker portion (in blue) is 2*a* and that of the thin portion (in yellow) is *a*. From mechanism point of view, the kinematic model in this four-crease thick-panel origami vertex is equivalent to a Bennett linkage of symmetric case. With $\varphi_i=\phi_i$ (i = 1, 2, 3, 4, see Figs. 1(a) and (b)), the equivalent folding performances of the four-crease zero-thickness rigid origami and the thick-panel form origami have been analyzed and verified in [32]. It should be pointed that, to form the equivalent Bennett linkage of one-DOF as shown in Fig. 1(b), the special geometry condition $\alpha+\beta=\pi$ must be satisfied.

In addition to the special case with $\alpha+\beta=\pi$ in Fig. 1(a), Fig. 1(c) gives the general plane-symmetric four-crease zero-thickness origami vertex with the condition that $\alpha+\beta<\pi$. In this case, under the definition of mountain crease and valley crease, such a vertex cannot be deployed to a planar state but can be folded flat. In this paper, we try to construct its corresponding thick-panel origami form that preserves the kinematics of the zero-thickness form. Firstly, we use the hinge shift technique having been applied to the Miura-ori pattern, as shown in Fig. 1(d), the corresponding thick-panel origami constructed by this method turns out to be a structure with no mobility, which can only be assembled in the fully folded configuration. This is due to the reason that the strict geometry constraints for forming a Bennett linkage are no longer satisfied as $\alpha+\beta\neq\pi$. In order to solve this problem and find an equivalent thick-panel counterpart for the general case of plane-symmetric four-crease origami, this paper proposes a new technique, which extends the hinge shift technique [26], the doubled-hinge method [24], and our previous work [32, 33].

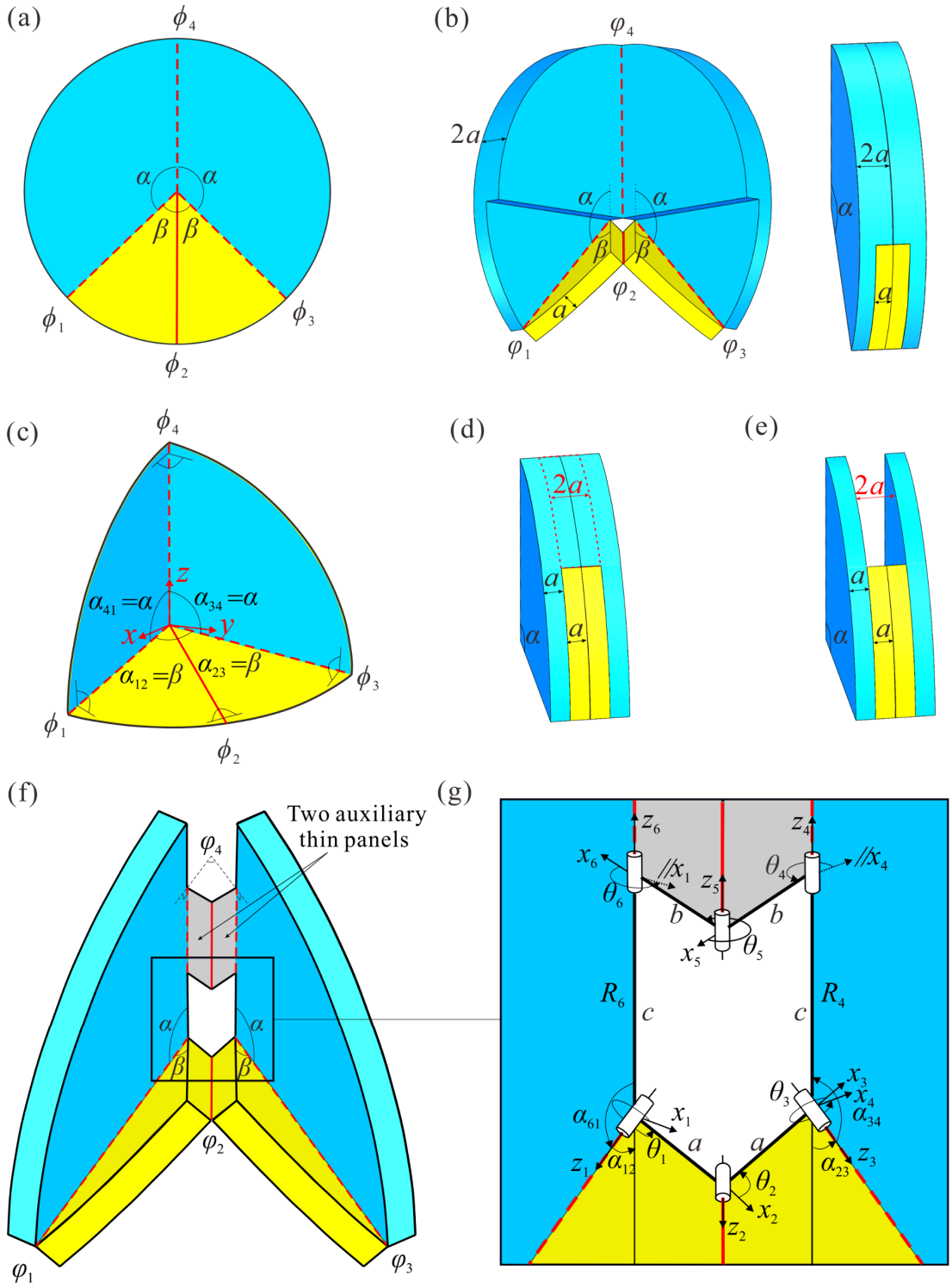

Fig. 1. Plane-symmetric four-crease zero-thickness origami vertices and the corresponding thick-panel forms. (a) The plane-symmetric origami vertex with $\alpha+\beta=\pi$ and (b) its thick-panel form in Miura-ori pattern. (c) The general plane-symmetric origami vertex with $\alpha+\beta<\pi$; (d) the corresponding thick-panel structure without mobility; (e) four panels in an overlapped state with a gap of $2a$; (f) the general plane-symmetric thick-panel origami vertex and (g) its equivalent plane-symmetric Bricard linkage.

Referring to the structure in Fig. 1(d), to make it an equivalent thick-panel mechanism, we remove the inner material of thickness a each respectively from the two

α sectors, as highlighted in red dotted area in Fig. 1(d). The structure then turns into the overlapped state with four panels of consistent thickness a, see Fig. 1(e). At this stage, a gap of $2a$ appears and thus a close-loop assembly cannot be formed since the two blue panels are not connected. To overcome this problem, referring to Fig. 1(f), we add two auxiliary thin panels (illustrated in grey) connected by three parallel revolute joints symmetrically between the two panels with sector angle α. These two panels are articulated by a revolute joint (with joint axis denoted as z_5 in Fig. 1(g)), and are connected to the two α-section thick panels by two other revolute joints (with joint axes denoted as z_4 and z_6, respectively in Fig. (1g)). Joint axes z_4 and z_6 are symmetric with respect to joint axis z_5. The plane-symmetric Bricard linkage can preserve the kinematics of the original zero-thickness origami, which is proven in the next section.

2.2 Kinematic equivalence

In this section, the kinematic analysis of general plane-symmetric origami vertex in Fig. 1(c) and proposed thick-panel form in Fig. 1(f) is carried out based on the matrix method with the D-H notations [35].

Firstly, the notation used for the analysis is introduced. For a part of a spatial linkage with revolute joints, see Fig. 2, z_i is along the axis of revolute joint i and x_i is along the direction of the common perpendicular between z_{i-1} and z_i. The geometrical parameter $a_{i(i+1)}$ represents the distance between z_i and z_{i+1}, also known as the length of link $i(i+1)$, positive along the axis x_{i+1}; $\alpha_{i(i+1)}$ represents the twist angle between z_i and z_{i+1} about the axis x_{i+1}; and offset R_i is the distance between axes x_i and x_{i+1} along the z_i axis. Further, the joint angle θ_i is defined as the rotation angle between x_i and x_{i+1} about the axis z_i, here it has $\theta_i \in (0, 2\pi)$ in this paper. In general, for a single-loop spatial linkage consisting of i links, the closure equation using the transformation matrices obtained through the D-H parameters is

$$\mathbf{T}_{21}\mathbf{T}_{32}...\mathbf{T}_{i(i-1)}\mathbf{T}_{1i} = \mathbf{I}_4 . \tag{1}$$

The transformation matrix $\mathbf{T}_{(i+1)i}$ can be expressed as

$$\mathbf{T}_{(i+1)i} = \begin{bmatrix} \cos\theta_i & -\cos\alpha_{i(i+1)}\sin\theta_i & \sin\alpha_{i(i+1)}\sin\theta_i & a_{i(i+1)}\cos\theta_i \\ \sin\theta_i & \cos\alpha_{i(i+1)}\cos\theta_i & -\sin\alpha_{i(i+1)}\cos\theta_i & a_{i(i+1)}\sin\theta_i \\ 0 & \sin\alpha_{i(i+1)} & \cos\alpha_{i(i+1)} & R_i \\ 0 & 0 & 0 & 1 \end{bmatrix}, \tag{2}$$

For a single-loop spherical linkage, the axes of revolute joints meet at a point, the lengths of each link are zero, and thus closure equation Eq. (1) reduces to

$$\mathbf{Q}_{21}\mathbf{Q}_{32}...\mathbf{Q}_{i(i-1)}\mathbf{Q}_{1i} = \mathbf{I}_3 \tag{3}$$

where

$$\mathbf{Q}_{(i+1)i}=\begin{bmatrix}\cos\theta_i & -\cos\alpha_{i(i+1)}\sin\theta_i & \sin\alpha_{i(i+1)}\sin\theta_i\\ \sin\theta_i & \cos\alpha_{i(i+1)}\cos\theta_i & -\sin\alpha_{i(i+1)}\cos\theta_i\\ 0 & \sin\alpha_{i(i+1)} & \cos\alpha_{i(i+1)}\end{bmatrix}. \tag{4}$$

Closure equations (1) and (3) can be used to obtain the relationships of the joint angles at each thick-panel origami vertex and rigid origami vertex, respectively.

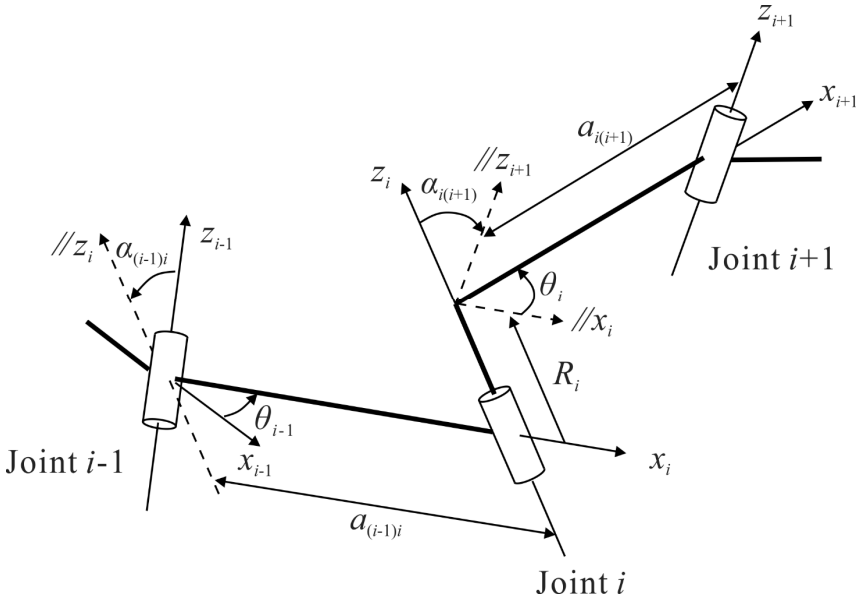

Fig. 2. The D-H notations of a portion of a spatial linkage.

Based on the above formulation, for the four-crease origami vertex in Fig. 1(c), its kinematics can be deduced through the equivalent spherical 4*R* linkage with the geometric parameters that $\alpha_{12}=\alpha_{23}=\beta$ and $\alpha_{34}=\alpha_{41}=\alpha$, the relationships between the dihedral angles and kinematic joint angles are $\phi_1=\theta_1-\pi$, $\phi_2=\pi-\theta_2$, $\phi_3=\theta_3-\pi$ and $\phi_4=\theta_4-\pi$. Substituting these geometric parameters into the D-H-convention-based closure equations, Eq. (3), the relationships of dihedral angles at this origami vertex can be expressed with respect to the sector angles α and β as

$$\tan\frac{\phi_2}{2}=\frac{\sin\alpha\sin\phi_1}{\sin\alpha\cos\beta\cos\phi_1-\cos\alpha\sin\beta}, \tag{5a}$$

$$\phi_3=\phi_1, \tag{5b}$$

$$\cos\phi_4=1+\frac{\sin^2\beta}{\sin^2\alpha}\left(\cos\phi_2-1\right), \tag{5c}$$

where ϕ_1 is taken as the input dihedral angle for the general plane-symmetric origami vertex.

Using Eq. (5) and specifying that the sector angles are $\alpha=\pi/2$ and $\beta=\pi/4$, the input-output curves relating the dihedral angles of the general plane-symmetric origami vertex can be obtained and illustrated in Fig. 3.

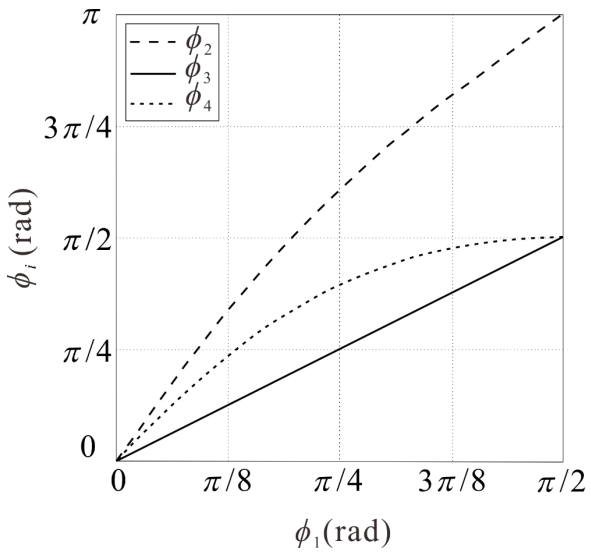

Fig. 3. Input-output curves of dihedral angles of the general plane-symmetric origami vertex with $\alpha = \pi/2$ and $\beta = \pi/4$.

For the derived thick-panel origami vertex in Fig. 1(f), its equivalent mechanism in a plane-symmetric Bricard linkage form is illustrated in Fig. 1(g), where the coordinate frames are established, and the associated D-H parameters are assigned. In addition, the D-H parameters of the proposed plane-symmetric Bricard linkage have the following relationships,

$$\begin{aligned} &\alpha_{12} = -\alpha_{23} = -\beta,\ \ \alpha_{34} = -\alpha_{61} = -\alpha, \alpha_{45} = \alpha_{56} = 0, \\ &a_{12} = a_{23} = a, a_{34} = a_{61} = 0, a_{45} = a_{56} = b\ , \\ &R_1 = R_2 = R_3 = R_5 = 0,\ \ R_4 = -R_6 = c, \end{aligned} \tag{6}$$

where link length a represents the thickness of the sector panels, and b is the width of the two auxiliary thin panels, offset c can be selected based on the structure of the proposed thick-panel with the condition that no interference during the motion being considered.

Substituting the above D-H parameters into the closure equation, Eq. (1), the joint angle relationships of the plane-symmetric Bricard linkage can be derived as

$$\tan\frac{\theta_2}{2} = \frac{\sin\alpha\sin\theta_1}{-\sin\alpha\cos\beta\cos\theta_1 + \cos\alpha\sin\beta}, \tag{7a}$$

$$\cos\frac{\theta_5}{2} = -\frac{a}{b}\cos\frac{\theta_2}{2}, \tag{7b}$$

$$\cos\left(2\theta_4 + \theta_5\right) = 1 + \frac{\sin^2\beta}{\sin^2\alpha}\left(\cos\theta_2 - 1\right), \tag{7c}$$

$$\theta_3 = \theta_1,\ \ \theta_6 = \theta_4, \tag{7d}$$

where θ_1 is the input for the one-DOF plane-symmetric Bricard linkage.

Referring to Fig. 1(f), the dihedral angles of the four sector panels are φ_1, φ_2, φ_3, and φ_4. Here, φ_4 is the virtual dihedral angle between the two panels with sector angle α. Comparing the thick-panel origami vertex in Fig. 1(f) and the equivalent Bricard linkage in Fig. 1(g), the dihedral angles can be expressed with respect to the joint angles as

$$\varphi_1 = \varphi_3 = 2\pi - \theta_1, \quad \varphi_2 = \theta_2, \tag{8a}$$

$$\varphi_4 = 2\pi - (\theta_4 - \frac{\pi}{2}) - (\theta_5 - \pi) - (\theta_6 - \frac{\pi}{2}) = 4\pi - 2\theta_4 - \theta_5. \tag{8b}$$

Substituting Eq. (8) into Eq. (7), with φ_1 being the equivalent input (related to input angle θ_1 of the equivalent Bricard linkage), the relationships of dihedral angles expressed by the sector angles α and β are

$$\tan\frac{\varphi_2}{2} = \frac{\sin\alpha\sin\varphi_1}{\sin\alpha\cos\beta\cos\varphi_1 - \cos\alpha\sin\beta}, \tag{9a}$$

$$\varphi_3 = \varphi_1, \tag{9b}$$

$$\cos\varphi_4 = \cos(2\theta_4 + \theta_5) = 1 + \frac{\sin^2\beta}{\sin^2\alpha}(\cos\varphi_2 - 1), \tag{9c}$$

which are consistent with relationships for the dihedral angles of the original zero-thickness origami vertex obtained in Eq. (5).

Hence, from the above derivation, we prove that the kinematic properties of the proposed thick-panel origami vertex are the same as the corresponding zero-thickness origami.

It should be noted that, due to the gap of $2a$ in the folded state of the thick-panel origami vertex, the width b of the auxiliary panels (see Fig. 1(g)) should satisfy the condition that $b/a \geq 1$. This ensures that the entire folding motion can be achieved. From Eq. (7), it can be seen that the angles θ_4, θ_5 and θ_6 are related to b/a, but in Eq. (9), it shows that the relationships among the dihedral angles φ_i in the thick-panel origami are not affected by b/a.

Further, by assigning that $\alpha = \pi/2$ and $\beta = \pi/4$, and $b/a = 1$ (or $b/a = \sqrt{2}$), and substituting the geometric parameters into Eqs. (7) and (9), the input-output curves for the joint angles of the equivalent plane-symmetric Bricard linkage, and for the dihedral angles of the associated thick-panel origami vertex are obtained and illustrated in Fig. 4. Comparing Fig. 4(b) with Fig. 3, it can be found that the relationships for the dihedral angles of the thick-panel form in Fig. 1(f) are identical with that of the corresponding zero-thickness origami in Fig. 1(c). Therefore, from the above analysis, the equivalence of their folding performances has been proven. It is noted that the two auxiliary panels in the thick-panel origami are connected by parallel joints and their further physical construction depends on the specific application. Overall, to secure the proposed design, according to the structure of the thick panel, the condition that $1 \leq b/a \leq \sqrt{1 + (c/a)^2 \tan^2(\alpha - \beta)}$ should always be considered to avoid physical interference.

For example, in the phototype shown in Fig. 5 (in which the sector angles are $\alpha = \pi/2$ and $\beta = \pi/4$ according to Figs. 1(f) and 1(g)), to make the position of axis z_5 stable and avoid bifurcation when z_4 and z_6 are collinear in the fully deployed state, right-angled isosceles triangular prism structures are adopted as the auxiliary panels, and in this case $b = \sqrt{2}a$.

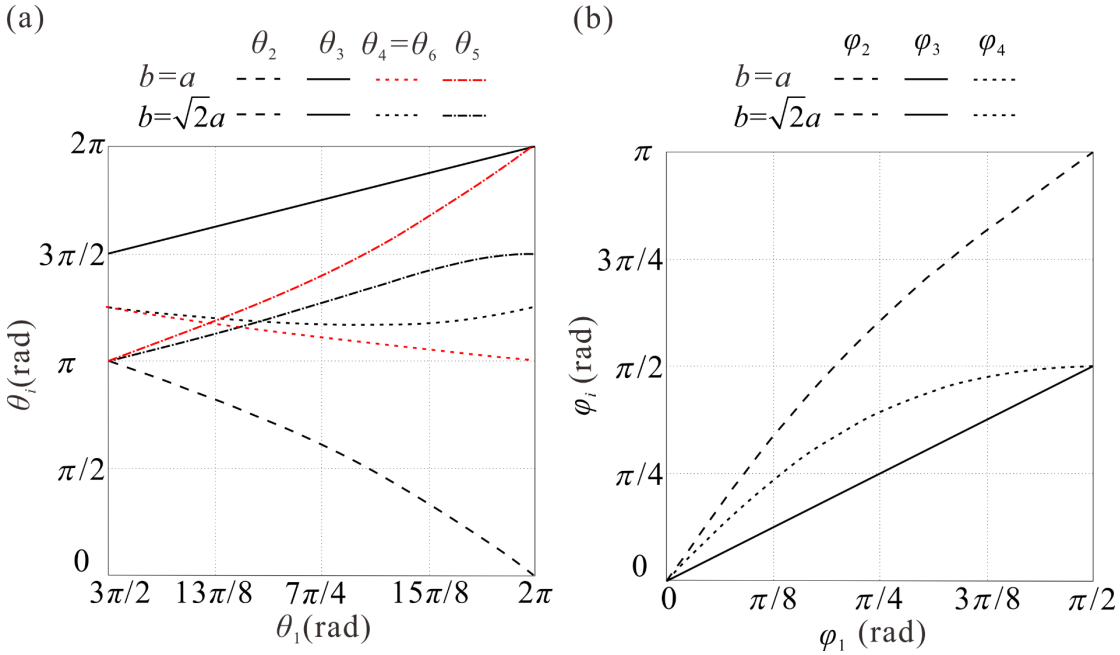

Fig. 4. Input-output curves of (a) joint angles θ_i in the Bricard linkage and (b) dihedral angles φ_i of the thick-panel origami vertex with $\alpha = \pi/2$, $\beta = \pi/4$ and $b/a = 1$ or $\sqrt{2}$.

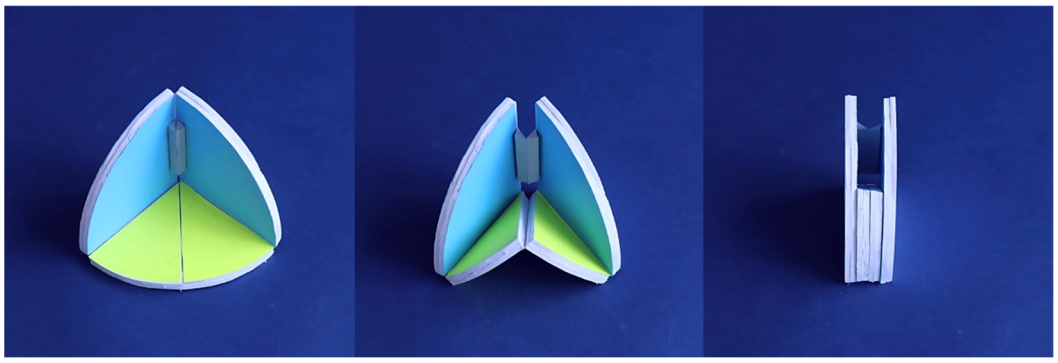

Fig. 5. Folding process of the general plane-symmetric thick-panel origami vertex.

Therefore, in this section, a novel thick-panel origami vertex with kinematic equivalence for the general plane-symmetric four-crease zero-thickness origami vertex is identified and constructed, which is equivalent to a plane-symmetric Bricard linkage, hence we call it a PSBL thick-panel origami vertex.

3 Construction and analysis of a thick-panel origami cube

A zero-thickness origami cube has been presented in our previous work [34], as shown in Fig. 6(a). In this crease pattern, there are three symmetric four-crease origami vertices A, B and C, and one symmetric six-crease vertex D, these vertices form a foldable 4*R*-4*R*-4*R*-6*R* spherical linkage loop, which has been proven to have the mobility of one and is flat foldable [34] (The detailed description and the kinematic analysis results of this zero-thickness origami cube are provided in Appendix A). In this section, by replacing the three plane-symmetric four-crease origami vertices with the proposed PSBL thick-panel origami vertex, we aim to construct a thick-panel origami cube that preserves the kinematics of the zero-thickness origami cube.

3.1 Construction of the thick-panel origami cube

Referring to Fig. 6(b), to construct a thick-panel origami cube, by placing the original zero-thickness origami cube in the deployed cube configuration, we replace the four-crease vertices A, B and C with the proposed PSBL thick-panel vertex, where the auxiliary panels are placed along edge AD, BF and CD, respectively. The PSBL vertices at vertices A and B share a common revolute joint along edge AB, and two common panels as triangular facets ABD and ABF. Similarly, the PSBL vertices at vertices B and C have a common joint along edge BC, and two common panels, i.e. triangular panels BCD and BCF. The three PSBL vertices at vertices A, B and C are of the identical geometry. Then, by merging the related joints and panels, and expanding the panels shapes, a think-panel form is constructed as illustrated in Fig. 6(c), in which the panels associated with vertex H and edge DH are missed. In order to generate a thick-panel cube, two additional triangular panels, i.e. panels DEH and DGH, are implanted connecting by revolute joints along edges DE and DG. If a revolute joint is used to connect panels DEH and DGH along edge DH, the thick-panel cube will become a structure.

To obtain the entire thick-panel cube with mobility one and flat foldability, similar as the construction of the PSBL vertex, we add another two auxiliary panels together with three parallel revolute joints along edge DH. Ultimately, a thick-panel origami cube is constructed as shown in Fig. 7. The proposed thick-panel cube in Fig. 7(a) contains 10 identical triangular panels and four pairs of auxiliary panels that are connected by 21 revolute joints. While vertices A, B, and C are 6*R* linkages, vertex D is formed by three edges (DA, DC, DH) with auxiliary panels with their associated joints and three diagonal revolute joints (DB, DE, DG), which is equivalent to a spatial 12*R* linkage. Hence, the whole thick-panel origami cube is equivalent to a 6*R*-6*R*-6*R*-12*R* integrated overconstrained linkages.

In the design of thick-panel origami cube in Fig. 7, considering the geometric conditions in the crease pattern of the original zero-thickness origami cube, right-angled isosceles triangular prism blocks are adopted as the auxiliary panels for the three PSBL thick-panel vertices as well as the two along edge DH. The width of the auxiliary panels for the three PSBL vertices is $\sqrt{2}a$, and width of the auxiliary panels along edge DH is $3\sqrt{2}a$, with a being the thickness of all triangular panels. It should be noted that the total width of the two identical auxiliary panels should be greater than the thickness of the internal six-layer panels in the folded state without interference, so the width b' of each auxiliary panel along edge DH should satisfy the condition that $3a \le b' \le \sqrt{9a^2 + (L-l)^2/4}$, in which L is the side length of the cube and l is the length of auxiliary panel. Similar to the design strategy of the auxiliary panels in the PSBL

vertices, to make the position of axis z_1 stable at vertex D (see Fig .8) at the fully deployed state and to avoid interference, we assign the width of the auxiliary panels (right-angled isosceles triangular prism blocks) along edge DH as $3\sqrt{2}a$.

In the following section, we prove that the proposed thick-panel cube can preserve kinematics of the original zero-thickness origami cube, both of mobility one.

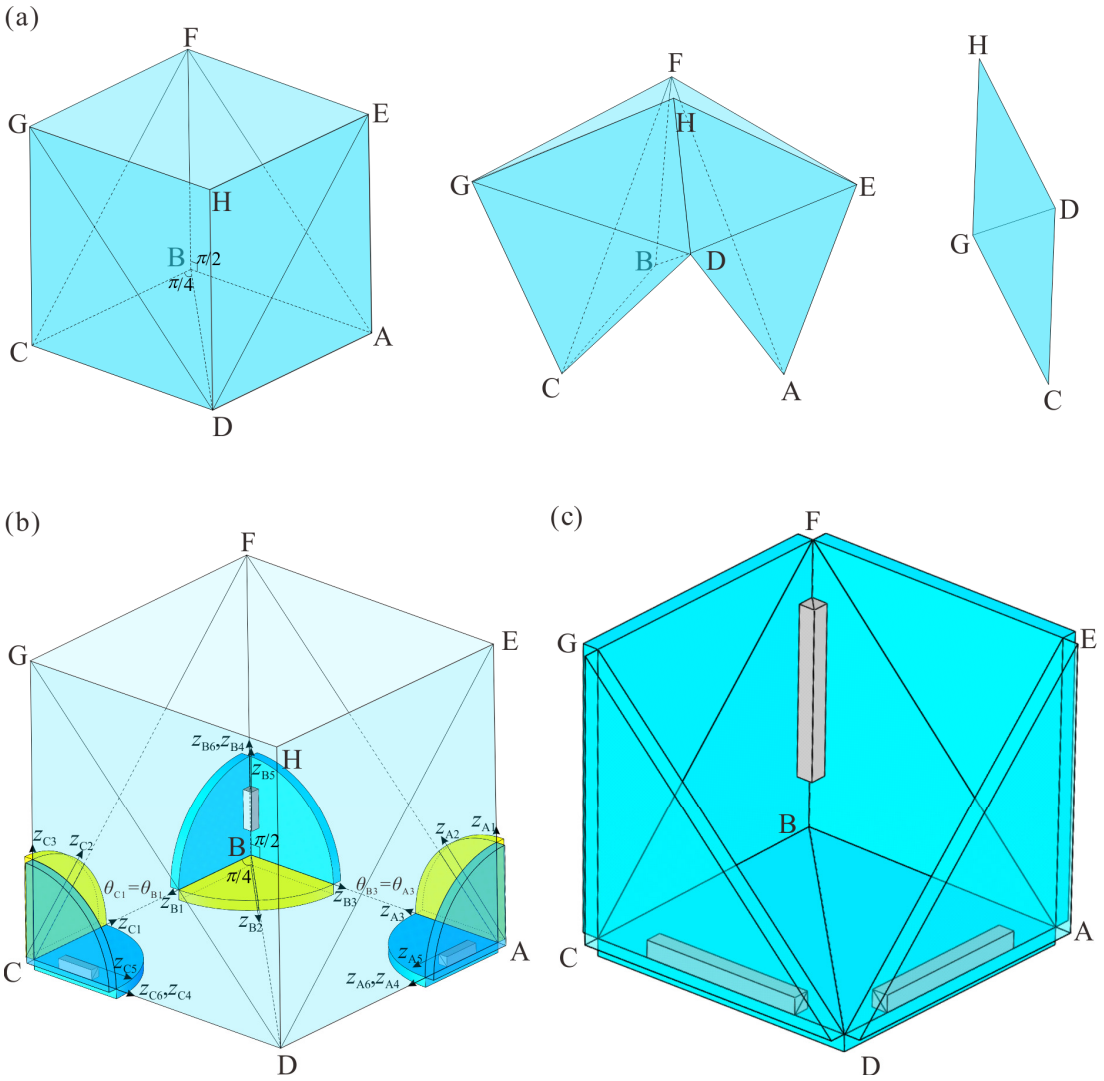

Fig. 6. Construction of thick-panel mechanism based on a zero-thickness origami cube. (a) Typical configurations of the zero-thickness origami cube [34]; (b) the integration of PSBL thick-panel vertices at vertices A, B and C; (c) a thick-panel form made by three PSBL think-panel vertices.

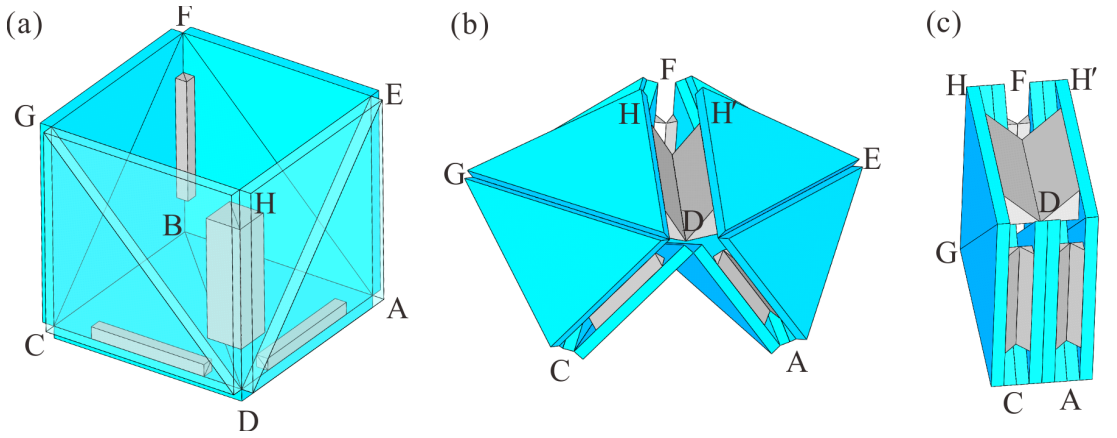

Fig.7. Thick-panel origami cube with 6*R*-6*R*-6*R*-12*R* integrated mechanism from (a) the deployed configuration, via (b) a middle configuration, to (c) the folded configuration.

3.2 Kinematics preservation

To carry out kinematic analysis of the proposed thick-panel origami cube, using mechanism decomposition, its equivalent 6*R*-6*R*-6*R*-12*R* integrated mechanism can be decomposed into four sub-linkages at the four vertices A, B, C and D. The three sub-linkages at vertices A, B and C are all equivalent to the plane-symmetric 6*R* Bricard linkage, and the sub-linkage at vertex D is a spatial 12*R* linkage. Kinematics of the plane-symmetric 6*R* Bricard linkage has been presented in Section 2, hence, kinematics of linkages A, B and C and be formulated straightforward by adapting the related derivation in Section 2.

The PSBL thick-panel vertices A, B and C have the same geometric parameters, $\alpha=\pi/2$, $\beta=\pi/4$ and $b=\sqrt{2}a$. Hence, with the coordinate frames shown in Fig. 6(b), by adapting Eq. (7), general relationships of the joint angles can be rewritten as

$$\begin{aligned}&\tan\frac{\theta_{i2}}{2}=-\sqrt{2}\tan\theta_{i1},\ \cos\frac{\theta_{i5}}{2}=-\frac{\sqrt{2}}{2}\cos\frac{\theta_{i2}}{2},\\&\cos\left(2\theta_{i4}+\theta_{i5}\right)=\frac{1}{2}\left(\cos\theta_{i2}+1\right),\ \theta_{i3}=\theta_{i1},\ \theta_{i6}=\theta_{i4},\end{aligned}\tag{10}$$

in which $i=$ A, B, C.

Thus the corresponding dihedral angles for the PSBL thick-panel vertices have the following relations,

$$\tan\frac{\varphi_{i2}}{2}=\sqrt{2}\tan\varphi_{i1},\ \ \varphi_{i3}=\varphi_{i1},\ \ \cos\varphi_{i4}=\frac{1}{2}\left(\cos\varphi_{i2}+1\right),\tag{11}$$

where $i=$ A, B, C.

In addition to the above relationships, due to the fact that each pair of the adjacent PSBL thick-panel vertices A, B and C shares a common revolute joint, referring to Fig. 6(b), there exit further relations that

$$\theta_{\mathrm{A3}}=\theta_{\mathrm{B3}},\ \ \theta_{\mathrm{B1}}=\theta_{\mathrm{C1}},\tag{12a}$$

and

$$\varphi_{A3} = \varphi_{B3}, \quad \varphi_{B1} = \varphi_{C1}. \tag{12b}$$

Hence, for the three PSBL thick-panel vertices A, B, and C and their equivalent linkages, the assembly conditions can be expressed as

$$\theta_{Aj} = \theta_{Bj} = \theta_{Cj} \quad (j=1, 2, ..., 6), \tag{13a}$$

and

$$\varphi_{Aj} = \varphi_{Bj} = \varphi_{Cj} \quad (j=1, 2, 3, 4). \tag{13b}$$

The thick-panel vertex D is indicated in Fig. 8, it contains six triangular panels and six auxiliary panels, that are connected by 12 revolute joints, it is equivalent to a spatial 12*R* linkage. This linkage is coupled with the plane-symmetric Bricard linkages at vertices A, B and C, hence to ensure the entire folding motion and the axis positions between auxiliary panels, link lengths in the 12*R* linkage at vertex D have the following relationships

$$\begin{aligned} &a_{D12} = a_{D12,1} = 3\sqrt{2}a, \ a_{D23} = a_{D34} = a_{D10,11} = a_{D11,12} = 0, \\ &a_{D45} = a_{D56} = a_{D89} = a_{D9,10} = \sqrt{2}a, \ a_{D67} = a_{D78} = a, \end{aligned} \tag{14a}$$

with the coordinate frames established in Fig. 8(b), other D-H parameters of this 12*R* linkage are identified as

$$\begin{aligned} &\alpha_{D12} = \alpha_{D45} = \alpha_{D56} = \alpha_{D89} = \alpha_{D9,10} = \alpha_{D12,1} = 0, \\ &\alpha_{D23} = \alpha_{D34} = \alpha_{D67} = \frac{\pi}{4}, \alpha_{D78} = \alpha_{D10,11} = \alpha_{D11,12} = -\frac{\pi}{4}, \\ &R_{D1} = R_{D3} = R_{D5} = R_{D7} = R_{D9} = R_{D11} = 0, \\ &-R_{D2} = R_{D4} = -R_{D6} = R_{D8} = -R_{D10} = R_{D12} = c. \end{aligned} \tag{14b}$$

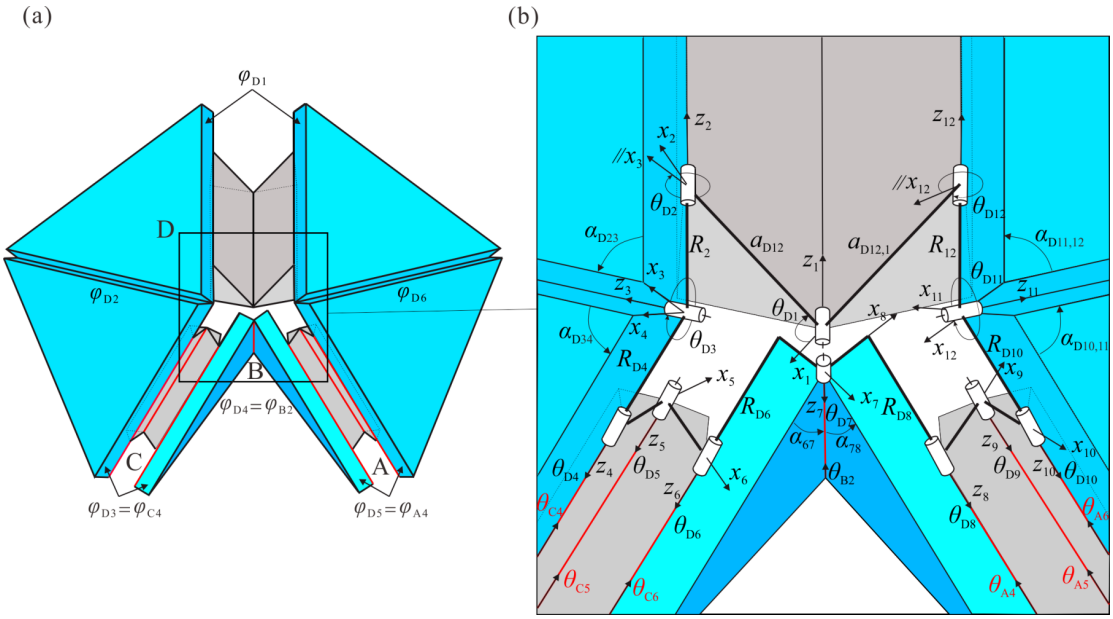

Fig. 8. Spatial 12*R* linkage at (a) vertex D and (b) its D-H coordinate frames.

Referring to Fig. 8(b), joint angles in the 12*R* linkage at vertex D that are coupled with the joints in the three Bricard linkages at vertices A, B and C can be related with the associated angles as follows. Related with linkage A, it has

$$\theta_{D8}=3\pi-\theta_{A4},\quad \theta_{D9}=2\pi-\theta_{A5},\quad \theta_{D10}=2\pi-\theta_{A6}, \tag{15a}$$

relating with linkage B, there exists

$$\theta_{D7}=2\pi-\theta_{B2}, \tag{15b}$$

and relating with linkage C, it has

$$\theta_{D4}=2\pi-\theta_{C4},\quad \theta_{D5}=2\pi-\theta_{C5},\quad \theta_{D6}=3\pi-\theta_{C6}. \tag{15c}$$

If θ_{A1} is given as the only input of the 6*R*-6*R*-6*R*-12*R* integrated mechanism, kinematics of the 6*R* linkages at vertices A, B and C can be determined by Eqs. (10), (12a) and (13a). Then, based on Eqs. (13a) and (15), the seven joint angles θ_{D4} throughout θ_{D10} at vertex D can be deduced and represented with respect to θ_{A1} as

$$\theta_{D4}=\theta_{D6}-\pi=\theta_{D8}-\pi=\theta_{D10}=2\pi-\theta_{A4},\quad \theta_{D5}=\theta_{D9}=2\pi-\theta_{A5},\quad \theta_{D7}=2\pi-\theta_{A2}. \tag{16}$$

Further, by substituting the D-H parameters in Eq. (14) and kinematic conditions in Eq. (16) into the closure equation Eq. (1), the other five joint angles in the 12*R* linkage at vertex D can be expressed by θ_{D4}, θ_{D5} and θ_{D7} as

$$\cos\frac{\theta_{D1}}{2}=\frac{\left[\begin{array}{l}\left(\sin\theta_{D4}+\sin\left(\theta_{D4}+\theta_{D5}\right)\right)\left(\cos^2\left(\theta_{D4}+\frac{\theta_{D5}}{2}\right)+1-F\right)\\ +E\left(\sqrt{2}\left(\cos\theta_{D4}+\cos\left(\theta_{D4}+\theta_{D5}\right)\right)-1\right)-\frac{\sqrt{2}}{2}\sin\left(2\theta_{D4}+\theta_{D5}\right)\end{array}\right]}{-6\sqrt{1-\cos^4\left(\theta_{D4}+\frac{\theta_{D5}}{2}\right)+\frac{E}{\sqrt{2}}\sin\left(2\theta_{D4}+\theta_{D5}\right)-F\sin^2\left(\theta_{D4}+\frac{\theta_{D5}}{2}\right)}}, \tag{17a}$$

$$\cos^2\left(\frac{\theta_{D1}}{2}+\theta_{D2}\right)=\cos^4\left(\theta_{D4}+\frac{\theta_{D5}}{2}\right)-\frac{E}{\sqrt{2}}\sin\left(2\theta_{D4}+\theta_{D5}\right)+F\sin^2\left(\theta_{D4}+\frac{\theta_{D5}}{2}\right), \tag{17b}$$

$$\tan\frac{\theta_{D3}}{2}=\left[\begin{array}{l}\cos\left(2\theta_{D4}+\theta_{D5}\right)-\frac{\sqrt{2}}{2}\tan\frac{\theta_{D7}}{2}\sin\left(2\theta_{D4}+\theta_{D5}\right)\\ -\sqrt{\begin{array}{l}\sqrt{2}\tan\frac{\theta_{D7}}{2}\sin\left(2\theta_{D4}+\theta_{D5}\right)\left(1-\cos\left(2\theta_{D4}+\theta_{D5}\right)\right)\\ +\tan^2\frac{\theta_{D7}}{2}\left(\cos\left(2\theta_{D4}+\theta_{D5}\right)+\frac{1}{2}\sin\left(2\theta_{D4}+\theta_{D5}\right)\right)\\ +\cos^2\left(2\theta_{D4}+\theta_{D5}\right)\end{array}}\end{array}\right]/\tan\frac{\theta_{D7}}{2}, \tag{17c}$$

$$\theta_{D11}=\theta_{D3},\quad \theta_{D12}=\theta_{D2}, \tag{17d}$$

where $E=\cos\theta_{D7}\sin\left(2\theta_{D4}+\theta_{D5}\right)/\sqrt{2}-\sin\theta_{D7}\sin^2\left(\theta_{D4}+\frac{\theta_{D5}}{2}\right)$, and $F=\sin\theta_{D7}\sin\left(2\theta_{D4}+\theta_{D5}\right)/\sqrt{2}+\cos\theta_{D7}\sin^2\left(\theta_{D4}+\frac{\theta_{D5}}{2}\right)$.

Using the above joint angles of the 12*R* linkage at vertex D, the dihedral angles between the adjacent triangular panels for the corresponding thick-panel vertex can be derived as

$$\varphi_{D1} = 2\theta_{D2} + \theta_{D1} - 4\pi\,, \tag{18a}$$

$$\varphi_{D2} = \varphi_{D6} = \theta_{D3} - \pi\,, \tag{18b}$$

$$\varphi_{D3} = \varphi_{D5} = 2\theta_{D4} + \theta_{D5} - 2\pi\,, \tag{18c}$$

$$\varphi_{D4} = 2\pi - \theta_{D7}\,. \tag{18d}$$

In addition, referring to Fig. 8(a), the dihedral angles at vertex D, i.e., φ_{D3}, φ_{D4} and φ_{D5} can also be obtained directly from the related dihedral angles in the PSBL thick-panel vertices A, B and C as

$$\varphi_{D3} = \varphi_{C4}\,,\quad \varphi_{D4} = \varphi_{B2}\,,\quad \varphi_{D5} = \varphi_{A4}\,. \tag{19}$$

Given the inputs θ_{A1} and φ_{A1} respectively, using Eqs. (10)-(13) and (15)-(19), the input-output curves of joint angles θ_{Di} in the 12*R* linkage and dihedral angles φ_{Di} in the corresponding thick-panel vertex at vertex D are computed and shown in Fig. 9. The input-output curves for the dihedral angles at vertex D shown in Fig. 9(b) are the same as that for the zero-thickness origami cube indicated in [34]. From the above analysis, it can be seen that θ_{A1} is the only input of the equivalent 6*R*-6*R*-6*R*-12*R* integrated mechanism, and the rest of joint angles can be determined with θ_{A1}. Hence, the proposed thick-panel origami cube is equivalent to a 6*R*-6*R*-6*R*-12*R* integrated mechanism and has mobility one. Furthermore, as shown in Fig. 10, compared with the results in Fig. A2 in Appendix A [34], the input-output curves of the dihedral angles in the proposed thick-panel cube are the same as those in the original zero-thickness origami cube. Therefore, the proposed thick-panel cube preserves the kinematics of the original zero-thickness origami cube.

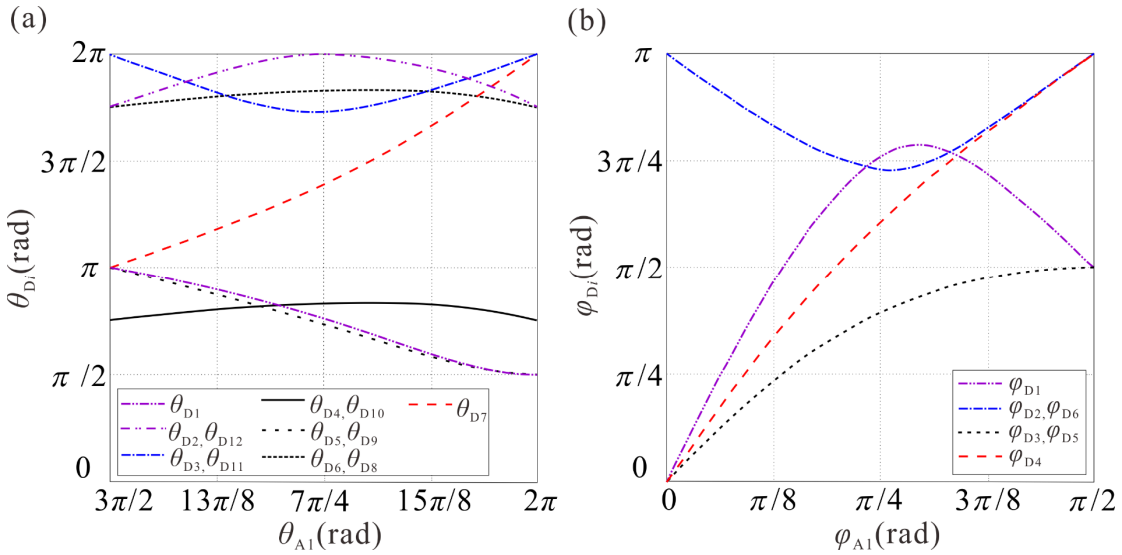

Fig. 9. Input-output curves of (a) joint angles θ_{Di} and (b) dihedral angles φ_{Di} in the spatial 12*R* linkage at vertex D.

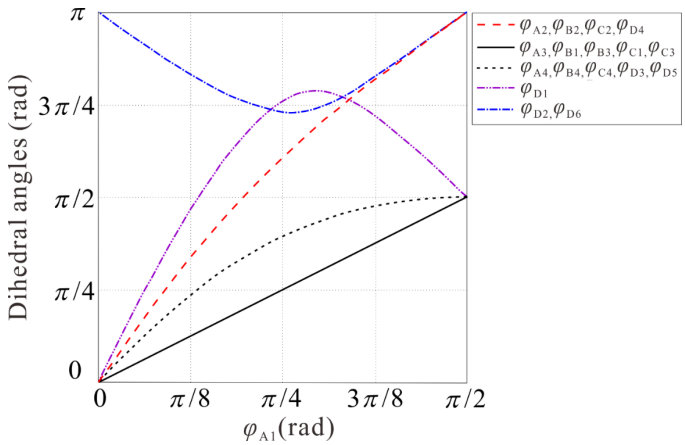

Fig. 10. Input-output curves of dihedral angles in the thick-panel origami cube.

3.3 Verification and extension

To verify the above design and analysis, a physical prototype of the proposed thick-panel cube is fabricated in this paper as shown in Fig. 11. The thick-panel cube is flat foldable, it can be fully expanded into a cube and folded into a flat block as shown in Fig. 11(a). It has mobility one and presents the plane-symmetric folding performance like the original zero-thickness origami cube. However, it should be pointed out that the top of this proposed thick-panel cube cannot be covered by additional thick panels to achieve flat foldability. This may be an open problem for further investigation. To seal the top of the proposed thick-panel cube, idealized zero-thickness facets (cardboard model) like the ones used for the origami cube in [34] can be temporarily employed, as shown in Fig. 11(b), the idealized zero-thickness top facets do not affect the folding performance of the proposed thick-panel cube.

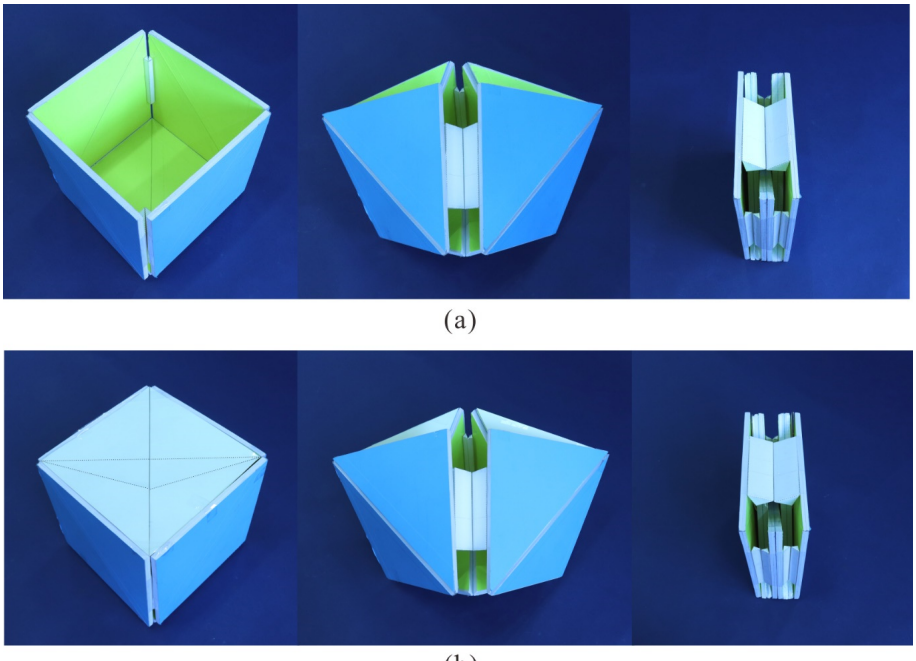

(a)

(b)

Fig. 11. Folding process of (a) thick-panel origami cube and (b) the model with origami top facets.

Further, referring to the construction of the proposed thick-panel origami cube, as shown in Fig. 12, the procedure of constructing thick-panel origami with kinematic equivalence based on a zero-thickness origami can be summarized as follows: Step 1, choose a zero-thickness origami crease pattern with general symmetric four-crease vertices; Step 2, replace each suitable zero-thickness four-crease vertex with the proposed PSBL thick-panel vertex; Step 3, synthesize thick-panel origami form based on crease pattern and verify the kinematic equivalence between thick-panel origami and zero-thickness form.

Based on kinematic equivalence, the kinematics of the original origami can be directly used to control and plan the motion of the evolved thick-panel origami-based structure in engineering applications. Noted that if the equivalent thick-panel origami form cannot be constructed in Step 3, the original zero-thickness crease pattern should be reconsidered.

For demonstration purpose, following the procedure of constructing equivalent thick-panel origami, a thick-panel cuboid is identified and constructed as follows to extend the application of the proposed synthesis approach. The zero-thickness crease pattern of a cuboid was presented in [15] (see Fig.13(a)), the zero-thickness origami cuboid can be fully expanded into a cuboid structure and be folded into a flat panel. In this crease pattern, vertices A, B, C and D are the symmetric four-crease origami vertices with the identical symmetric geometry, which have been given in [15]. These vertices can be conveniently replaced by the proposed PSBL thick-panel vertices. Through thick-panel transition at each vertex, Fig.13(b) shows the thick-panel cuboid structure with PSBLs at vertices A, B, C and D, in which the auxiliary panels are placed along edge AB and CD, respectively. Each pair of adjacent PSBL vertices share a common edge, i.e., AB, BC, CD and DA. The flat foldability and equivalent folding motion are preserved in the thick-panel cuboid.

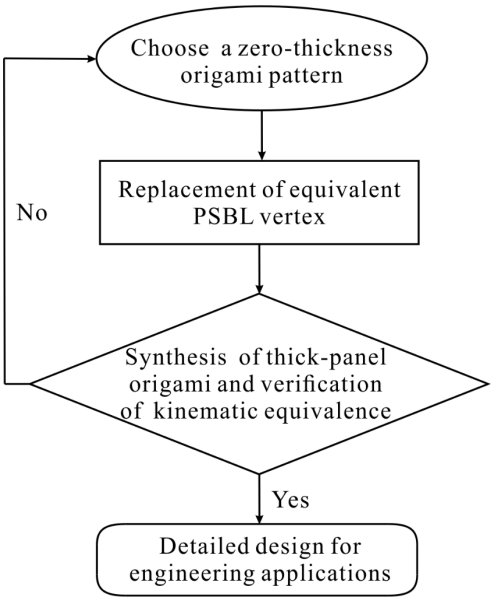

Fig. 12 The procedure of constructing equivalent thick-panel origami.

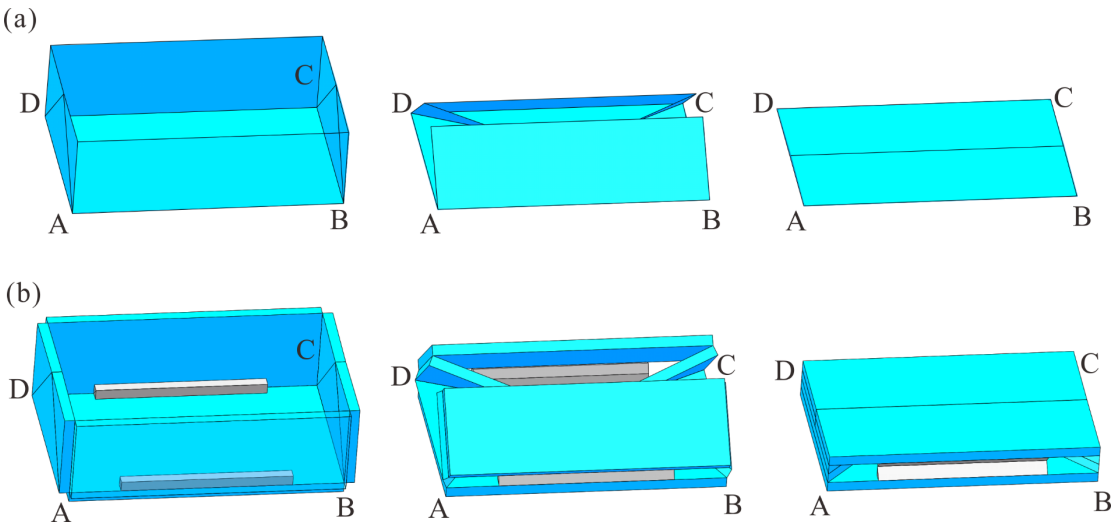

Fig. 13 Construction and folding process of deployable cuboid structure. (a) zero-thickness crease pattern [15]; and (b) corresponding thick-panel form with PSBL thick-panel vertices.

4. Conclusions and discussion

In this paper, we proposed an innovative approach for constructing a thick-panel origami cube. For a general plane-symmetric four-crease rigid origami vertex, a plane-symmetric Bricard linkage has been introduced and analysed to present the equivalent folding motion between the zero-thickness origami vertex and its thick-panel form. Using the proposed PSBL thick-panel origami vertex, the construction of a novel thick-panel origami cube of one-DOF was presented, and the geometric constraints and kinematic properties of its equivalent 6*R*-6*R*-6*R*-12*R* integrated mechanism have been investigated. It should be noted that, compared with original 4*R*-4*R*-4*R*-6*R* zero-thickness origami cube, the symmetric and equivalent motion behavior is completely preserved in this thick-panel form. Physical prototypes have been fabricated to demonstrate and verify the proposed thick-panel origami and the approach.

It is found that, in order to construct an equivalent PSBL thick-panel vertex, two pairs of symmetric sector angles of thick panels should be satisfied, and the symmetric condition between the two auxiliary panels with three parallel revolute joints should be met. For a zero-thickness origami crease pattern with general symmetric four-crease vertices, the proposed PSBL thick-panel vertex can be useful for the construction of its equivalent thick-panel form with the same geometry, which can reproduce identical motions and be readily applied to engineering applications.

In addition to constructing a thick-panel origami cube, the new method can be readily extended to transfer the zero-thickness origami patterns into its thick-panel counterpart, such as prism structures. Moreover, there are enriched designs of zero-thickness origami patterns cumulated in art and mathematics. It will be a great resource for engineering if we can take the original origami pattern directly and transfer it into the thick-panel form by keeping their folding motion equivalently by employing the

method proposed in this report; it will save engineers a lot of efforts in dealing with the compatibility for those independently proposed thick-panel origami patterns without referring to the original zero-thickness ones.

Acknowledgements

The authors would like to thank the financial support from the Natural Science Foundation of China (Projects No. 51825503, 52035008 and No. 51721003).

Appendix A: The zero-thickness origami cube [34]

The crease pattern of a zero-thickness origami cube in our previous work [34] is shown in Fig. A1. There are three symmetric four-crease origami vertices A, B and C with identical geometry, and one symmetric six-crease vertex D, which form a foldable 4*R*-4*R*-4*R*-6*R* spherical linkage loop. The dihedral angles of the zero-thickness origami cube are noted as φ_{ij} in [34]. As each pair of adjacent spherical linkages share a common joint, the kinematic relationships of dihedral angles are $\varphi_{A1}=\varphi_{B1}$, $\varphi_{B3}=\varphi_{C3}$, $\varphi_{C4}=\varphi_{D2}$, $\varphi_{D6}=\varphi_{A4}$ and $\varphi_{B2}=\varphi_{D1}$. If φ_{A1} is given as an input dihedral angle, the kinematics of three one-DOF S4*R* linkages are determined. Meanwhile, three inputs, φ_{D1}, φ_{D2} and φ_{D6}, required by three-DOF S6*R* linkage can also be obtained from φ_{B2}, φ_{C4} and φ_{A4}, respectively. The input-output curves of dihedral angles in Fig. A2 demonstrate that all dihedral angles can be determined with φ_{A1}. Hence, the zero-thickness origami cube with 4*R*-4*R*-4*R*-6*R* spherical linkage loop has mobility one.

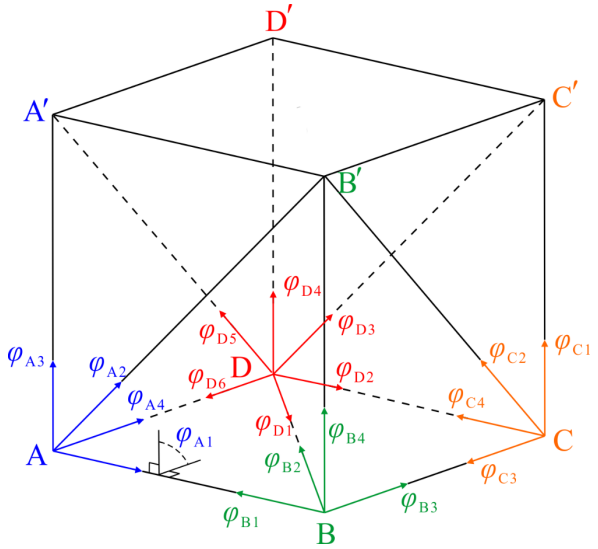

Fig. A1. The crease pattern and dihedral angles φ_{ij} of the zero-thickness origami cube [34].

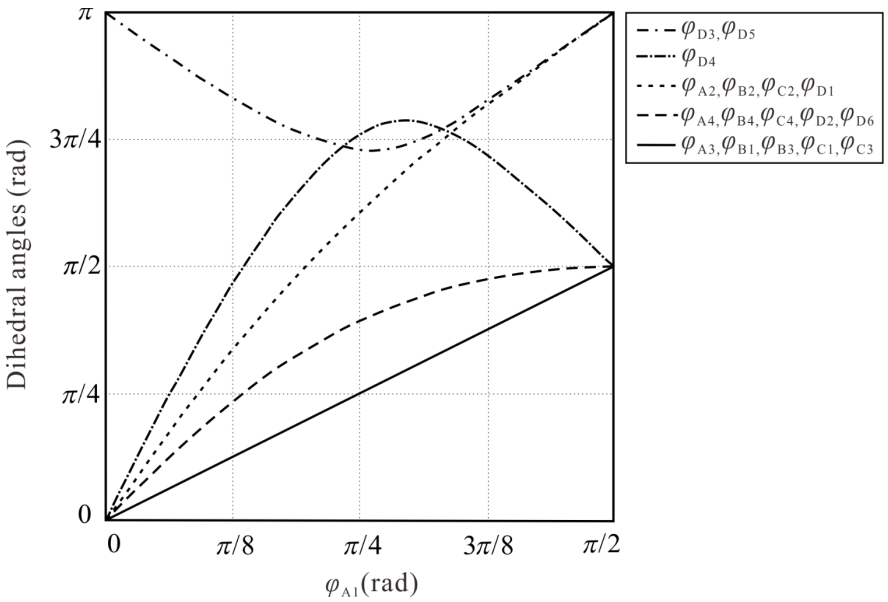

Fig. A2. Input-output curves of dihedral angles in the zero-thickness origami cube [34].

References

[1] L. Wilson, S. Pellegrino, R. Danner, Origami sunshield concepts for space telescopes, in: 54th AIAA/ASME/ASCE/AHS/ASC Structures, Structural Dynamics, and Materials Conference, 2013, p. 3013-1594. Boston, Massachusetts, USA.

[2] J. Morgan, S.P. Magleby, L.L. Howell, An approach to designing origami-adapted aerospace mechanisms, ASME J. Mech. Des. 138 (5) (2016) p. 052301.

[3] S. Felton, M. Tolley, E. Demaine, D. Rus, R. Wood, A method for building self-folding machines, Science 345 (6197) (2014) 644-646.

[4] S. Miyashita, S. Guitron, K. Yoshida, S. Li, D.D. Damian, D. Rus, Ingestible, controllable, and degradable origami robot for patching stomach wounds, in: 2016 IEEE International Conference on Robotics and Automation (ICRA), Stockholm, Sweden, 2016, pp. 909–916.

[5] K. Kuribayashi, K. Tsuchiya, Z. You, D. Tomus, M. Umemoto, T. Ito, M. Sasaki, Self-deployable origami stent grafts as a biomedical application of Ni-Rich TiNi shape memory alloy foil, Mater. Sci. Eng.: A 419 (1–2) (2006) 131-137.

[6] J.L. Silverberg, A.A. Evans, L. McLeod, R.C. Hayward, T. Hull, C.D. Santangelo, I. Cohen, Using origami design principles to fold reprogrammable mechanical metamaterials, Science 345 (6197) (2014) 647-650.

[7] H. Fang, S.C.A. Chu, Y. Xia, K.W. Wang, Programmable self-locking origami mechanical metamaterials, Adv. Mater. 30 (2018) 1706311.

[8] J. Song, Y. Chen, G. Lu, Axial crushing of thin-walled structures with origami patterns, Thin-Walled Struct. 54 (2012) 65-71.

[9] J. Ma, Z. You, Energy absorption of thin-walled square tubes with a prefolded origami pattern—Part I: geometry and numerical simulation, ASME J. Appl. Mech.

81(1) (2014) 011003.

[10] J.M.Z. Ocampo, P.O. Vaccaro, T. Fleischmann, T.S. Wang, K. Kubota, T. Aida, T. Ohnishi, A. Sugimura, R. Izumoto, M. Hosoda, S. Nashima, Optical actuation of micromirrors fabricated by the micro-origami technique, Appl. Phys. Lett. 83 (18) (2003) 3647-3649.

[11] J. Rogers, Y. Huang, O.G. Schmidt, D.H. Gracias, Origami MEMS and NEMS, MRS Bull. 41 (2) (2016) 123-129.

[12] K. Wang, Y. Chen, in: P Wang-Iverson, RJ Lang, M Yim (Eds.), Folding a patterned cylinder by rigid origami, Origami 5, AK Peters/CRC Press, New York, NY, 2011, pp. 265–276.

[13] J.S. Dai, J. Rees Jones, Mobility in metamorphic mechanisms of foldable/erectable kinds, J. Mech. Des. 121 (1999) 375–382.

[14] S. Liu, Y. Chen, G. Lu, The rigid origami patterns for flat surface, ASME 2013 International Design Engineering Technical Conferences and Computers and Information in Engineering Conference Portland, OR, 2013, V06BT07A039.

[15] Y. Chen, W. Lv, R. Peng, G. Wei, Mobile assemblies of four-spherical-4R-integrated linkages and the associated four-crease-integrated rigid origami patterns. Mech. Mach. Theory 142 (2019) 103613.

[16] G. Wei, J.S. Dai, Origami-inspired integrated planar-spherical overconstrained mechanisms, J. Mech. Des. 136 (5) (2014) 051003.

[17] R.J. Lang, K.A. Tolman, E.B. Crampton, S.P. Magleby, L.L. Howell, A review of thickness-accommodation techniques in origami-inspired engineering, Appl. Mech. Rev. 70 (2018) 010805.

[18] J.S. Dai, J.R. Jones, Kinematics and mobility analysis of carton folds in packing manipulation based on the mechanism equivalent, Proc. Inst. Mech. Eng. Part C 216 (2002) 959–970.

[19] T. Tachi, in: P Wang-Iverson, RJ Lang, M Yim (Eds.), Rigid-foldable thick-panel origami, Origami 5, A K Peters/CRC Press, New York, NY, 2011, pp. 253–264.

[20] M.R. Morgan, R.J. Lang, S.P. Magleby, L.L. Howell, Towards developing product applications of thick origami using the offset panel technique, Mech. Sci., 7 (2016) 69-77.

[21] B.J. Edmondson, R.J. Lang, M.R. Morgan, S.P. Magleby, L.L. Howell, Thick rigidly foldable structures realized by an offset panel technique, Origami6, American Mathematical Society, Providence, RI, 2015, pp. 149–161.

[22] K.A. Tolman, R.J. Lang, S.P. Magleby, L.L. Howell, Split-vertex technique for thickness-accommodation in origami-based mechanisms, ASME 2017 International Design Engineering Technical Conferences and Computers and Information in Engineering Conference Ohio, USA, 2017, V05BT08A054.

[23] J. Cai, Kinematic analysis of foldable plate structures with rolling joints, J. Mech. Rob. 8 (2016) 034502.

[24] J. S. Ku, E. D. Demaine, Rigid folding analysis of offset crease thick folding, IASS Annual Symposium on Spatial Structures in the 21st Century, Tokyo, Japan, 2016, Paper No. 1431.

[25] R.J. Lang, N. Brown, B. Ignaut, S. Magleby, L.L. Howell, Rigidly foldable thick-panel origami using designed-offset linkages, J. Mech. Rob. 12 (2020) 021106.

[26] C. Hoberman, Reversibly expandable three-dimensional structure, US Patent no. 4780344, 1988.

[27] G. Bennett, A new mechanism, Engineering 76 (1903) 777–778.

[28] C. Hoberman, Folding structures made of thick hinged sheets, US Patent no.7794019, 2010.

[29] Y. Chen, R. Peng, Z. You, Origami of thick panels, Science 349 (2015) 396–400.

[30] F.E. Myard, Contribution à la géométrie des systèmes articulés, Bull. Soc. Math. France 59 (1931) 183–210.

[31] R. Bricard, Leçons De cinématique, T. II, Gauthier-Villars, Paris, 1927.

[32] X. Zhang, Y. Chen, Mobile assemblies of Bennett linkages from four-crease origami patterns, Proc. R. Soc. A (2018) 474.

[33] X. Zhang, Y. Chen, The diamond thick-panel origami and the corresponding mobile assemblies of plane-symmetric Bricard linkages, Mech. Mach. Theory 130 (2018) 585-604.

[34] Y. Gu, Y. Chen, Origami cubes with one-DOF rigid and flat foldability, Int. J. Solids Struct. 207 (2020) 250-261.

[35] J. Denavit, R.S. Hartenberg, A kinematic notation for lower-pair mechanisms based on matrices, Trans. ASME J. Appl. Mech. 22 (1955) 215–221.